Advances in Science and Technology Research Journal

Advances in Science and Technology Research Journal, 2026, 20(3), 161–180
https://doi.org/10.12913/22998624/213938
ISSN 2299-8624, License CC-BY 4.0

Received: 2025.09.16
Accepted: 2025.11.04
Published: 2026.02.01

Dynamic behavior and vibration analysis of hybrid composite laminates reinforced with natural and carbon fibers for aeronautical applications using optical methods

Mebarki Abd Elyamine[1,2], Toufik Benmansour[1], Valéry Valle[3], Houssem Eddine Fiala[4*]

[1] Mechanical Engineering Department, Université Constantine 1, 25000, Constantine, Algeria
[2] Laboratory of Applied Mechanics and Energy Systems, Faculty of Applied Science, University of Kasdi Merbah, Ouargla, Algeria
[3] Institut Pprime. CNRS, Université de Poitiers, ENSMA. Boulevard Marie et Pierre Curie, BP 30179, Futuroscope Chasseneuil Cedex 86962, France
[4] Center of Research in Mechanics (CRM), 25000, Constantine, Algeria
* Corresponding author's e-mail: houssemeddine.fiala@umc.edu.dz

ABSTRACT

This work explores the dynamic behavior of hybrid composite laminates reinforced with natural and carbon fibers, with a focus on their potential use in aeronautical structures requiring lightweight and high-performance materials, experimental and numerical investigations were performed on composite plates reinforced with natural fibers (glass/ natural fibers /epoxy and natural fibers/epoxy) and benchmarked against conventional magnesium alloys and carbon fiber reinforced plastics (CFRP), using advanced optical techniques and LMS vibration testing systems at the PPRIM Institute (Poitiers, France), the vibrational response of specimens with varying thicknesses was analyzed under free-free boundary conditions (for natural frequency and mode shape identification) and constrained conditions (to simulate operational constraints), the moiré method provided non-destructive and contactless measurements of out-of-plane displacements, results reveal that thin natural fiber reinforced plates (FRN) can achieve frequencies and mode shapes comparable to magnesium alloys and CFRP, while highlighting differences between material systems, these findings demonstrate that FRN-based hybrid composites offer promising vibration characteristics for aeronautical applications, combining structural efficiency with enhanced sustainability.

Keywords: natural fiber reinforcement, optical methods, modal analysis, advanced composite materials, non-destructive testing.

INTRODUCTION

In recent decades, the rapid advancement of technology has led to an increased demand for high-performance dynamic testing methods, these methods are crucial for evaluating a wide range of products, from small, printed circuit boards to military equipment and satellites, vibration testing primarily serves to assess the dynamic behavior of components by measuring specific vibrational characteristics, which are essential for ensuring reliability and performance, vibration testing is typically employed for three main purposes: first, as a technical tool for design qualification, where vibrational characteristics such as natural frequencies and mode shapes are measured, these parameters are then used to develop or validate mathematical models of the design. Second, dynamic tests are conducted to evaluate reliability and fatigue life, often through accelerated life cycle tests to predict product lifespan within a short timeframe, Lastly, production lines utilize vibration testing as a screening method to identify defects prior to consumer sales, Given

these applications, there is ongoing research into realistic testing methods that can facilitate accurate laboratory simulations [1–2].

The mobile mass and structural stiffness of the testing system are critical for effective vibration testing. A lower moving mass requires less force for dynamic testing, while a higher stiffness combined with reduced weight generally leads to increased first vibration modes, thereby expanding the frequency bandwidth of tests, an ideal testing system would be constructed from materials that are both rigid and lightweight. However, for isotropic materials, these two properties are often mutually exclusive. Currently, the vibration testing industry primarily relies on isotropic metals for technical design. There is, however, a growing interest in advanced composite materials to enhance the performance of vibration testing systems due to their customizable properties and favorable stiffness-to-weight ratios.

Natural fiber reinforced composites (FRN) exhibit densities comparable to fiber-reinforced polymers (FRP), magnesium, and aluminum, yet can be engineered for significantly higher stiffness [3–4], composite materials offer greater design flexibility, allowing engineers to optimize shapes for maximum rigidity, the ease of forming these materials into complex shapes means that engineers are no longer limited to traditional plate and beam structures, with appropriate design, composites can achieve much higher stiffness-to-weight ratios than aluminum and magnesium. Given the advantages of FRN materials, the vibration testing industry is increasingly exploring structural components made from CFRN. These components, such as actuator head extenders for vertical tests and the moving plate of a sliding table for horizontal tests, are crucial for overall system performance as they effectively transfer energy from the actuator or shaker to the test specimen.

Recent studies have also explored the role of machining precision, micro-milling, and tool geometry in improving material performance under dynamic conditions, for instance, Rathod and Wankhade [13,14] provided comprehensive reviews on the impact of micro-tools and tool treatments on micro-milling outcomes for aluminum alloys, emphasizing precision and surface quality improvements relevant to dynamic structures. Kamble et al. [15] introduced the use of artificial neural networks (ANN) for optimizing center drill geometry in friction drilling of aluminum 6063, while Rathod et al. [16] experimentally analyzed process parameters in micro-milling of AA6063-T6 using cobalt WC tools. Furthermore, a comparative study by Rathod, Wankhade, and Kamble [17] evaluated the efficiency of micro end mill tools and performance metrics, highlighting the importance of tool selection in achieving enhanced vibrational and mechanical behavior, In addition, Boudjaada et al. [12] conducted an experimental and numerical investigation on the influence of honeycomb structures on the dynamic characteristics of rotors using modal analysis, their study demonstrated how lightweight core geometries can significantly alter stiffness distribution and modal responses, offering valuable insights for vibration optimization in composite systems, these studies collectively demonstrate how advances in machining and material processing contribute to the reliability and performance of high-frequency components used in dynamic systems.

A review of the literature highlights various types of dynamic analysis for composite materials, driven by the demand for high-performance materials in aerospace and marine structures [5]. More recently, several studies have reinforced this trend. A detailed review reported the mechanical and vibrational properties of natural fiber composites, with a focus on natural frequencies, damping ratio, and dynamic durability [6]. Impact testing demonstrated that these materials can exhibit excellent damping capabilities, which are vital for vibration control [7], non-destructive free vibration measurements were also employed to determine the elastic properties of jute/glass composites, validating the relevance of modal approaches [8], other studies emphasized the influence of free vibration behavior on natural and hybrid composites, highlighting the interplay of modal responses and damping effects [9], additional investigations revealed that fiber length and moisture content significantly affect the vibrational and acoustic responses of epoxy/hemp composites [10], complementing these findings, recent reviews have examined hybrid natural fiber composites, focusing on their mechanical, storage, and damping moduli, while underlining challenges related to stability and dynamic performance [11].

The future of research into composite materials, including FRP and biomimetic fibers,

is promising. Natural frequency analysis and the properties of composite plates have been studied for over 40 years, with the combination of different materials utilized for millennia to achieve superior performance requirements. Today, numerous applications across aerospace and automotive industries continue to expand the use of composite materials, now extending into sectors such as marine, sports goods, civil construction, and aerospace, understanding the effects of different parameters on natural frequency remains critical.

In this study, we focus on the vibrational characteristics of composite plates made from natural fibers reinforced with polyester, a topic that has been largely overlooked in existing research, by examining these panels under free-free boundary conditions, we investigate the effects of key factors such as the number of layers, fiber orientation angle, and aspect ratio on natural frequency, in contrast, panels made of fiberglass and carbon fiber are well-documented in the literature, known for their high strength-to-weight ratios and robust performance in vibration applications, while fiberglass offers good durability and cost-effectiveness, carbon fiber excels in stiffness and lightweight properties. However, these synthetic materials often come with environmental drawbacks and higher production costs, our research aims to highlight the advantages of natural fiber composites, which not only provide a sustainable alternative but also possess unique properties that can lead to competitive performance in vibration applications. By comparing these natural fibers with fiberglass and carbon fiber, we seek to demonstrate their potential for innovative engineering solutions that prioritize both performance and environmental responsibility.

Vibrations of symmetric orthotropic plates

A symmetric and balanced laminate is defined as having the same fiber orientation in the stacking sequence above and below the geometric mid-plane of the laminate. For each layer at angle θ, there exists a corresponding layer at angle -θ, these conditions fully decouple in plane stresses and curvatures. resulting in normal or shear stresses only when subjected to normal or shear loads. respectively. Moreover, the symmetric laminate condition ensures that thermal moments and moisture moments are always zero.

For a symmetric orthotropic laminate. the governing equation for free vibration is given by:

$$D_{11}\frac{\partial^4 w}{\partial x^4} + 4D_{16}\frac{\partial^4 w}{\partial x^3 y} + \\ + 2(D_{12} + 2D_{66})\frac{\partial^4 w}{\partial x^2\,\partial y^2} + 4D_{26}\frac{\partial^4 w}{\partial x\,\partial y^3} \\ + D_{22}\frac{\partial^4 w}{\partial y^4} + \rho h\frac{\partial^2 w}{\partial t^2} = 0 \quad (1)$$

where: (x, y, t) – displacement, D_{ij} – flexural rigidity coefficients of the laminate, ρ – density of the composite plate, x, y – total thickness of the laminate, t – time.

w $(x.y)$ represents the transverse displacement of the plate, h is the plate thickness, and Dij are the components of the bending stiffness matrix from classical laminate theory (CLT) defined as:

$$[D] = \int_{-\frac{h}{2}}^{\frac{h}{2}} z^2[\bar{Q}]\,dz \quad (2)$$

$$[D] = \int_{-\frac{h}{2}}^{\frac{h}{2}} z^2[\bar{Q}]^k\,dz = \\ = \frac{1}{3}\sum_{k=1}^{N}[\bar{Q}]^k(z_k^3 - z_{k-1}^3) \quad (3)$$

where: $[\bar{Q}]^k$ – is the transformed reduced stiffness matrix of the k[th] lamina, incorporating the effects of fiber orientation,
z_k – denote the top and bottom coordinates of the k[th] ply measured from the mid-plane of the laminate, N – is the total number of layers.

For especially orthotropic laminates, where three perpendicular planes of symmetry exist. D16=D26=0. simplifying Equation 1 to:

$$D_{11}\frac{\partial^4 w}{\partial x^4} + 2(D_{12} + 2D_{66})\frac{\partial^4 w}{\partial x^2 \partial y^2} + \\ + D_{22}\frac{\partial^4 w}{\partial y^4} + \rho h\frac{\partial^2 w}{\partial t^2} = 0 \quad (4)$$

For various plate conditions other than simply supported cases. solutions can become quite complex. if they can be determined at all, thus, a vibrational analysis must utilize an assumed displacement function. A common method for vibration problems is the Rayleigh-Ritz method. which employs the principle of minimum potential energy to find an approximate solution [18–19].

METHODOLOGY AND EXPERIMENTAL PROCEDURES

Materials

The materials tested in this research consist of composite plates made from woven glass/epoxy and natural fibers (Diss)/polyester, all with a thickness of less than 5 mm. The reinforced fiber naturel (RFN) plate was fabricated using 12 k 2 × 2 twill weave glass fabric, combined with a thermosetting epoxy resin as the matrix material. The dry areal density of the RFN was measured at 671 g/m².

Four RFN plate specimens (I. II. IV. and V) were produced using Orthotropic laminates. In selecting the types of plates for construction and testing, woven glass/epoxy composite plates were chosen. Four woven glass/epoxy composite plates were prepared for hand lay-up.

The maximum length of the plates is 300 mm, and the average thickness of all samples was measured using a micrometer with a minimum resolution of 0.01 mm, the fibers in each laminate are oriented at angles of 0°. 90°. +45°. and -45°, composites in this configuration are characterized in the loading plane by only two elastic constants, similar to orthotropic materials, an RFN plate (specimen III) is arranged in a cross-laminated configuration.

Table 1 presents the material properties for each of the two material systems utilized in this experiment. It is noteworthy that the properties of the RFN are specified for the tested condition [20]. Additionally, the natural fiber used in this study is Fiber DISS (F Diss) Figure 1.

The dimensions of the specimens were selected to represent a scaled model of a typical plate used in vibration testing and fastening applications. with a length of 300 mm. The specimens feature a square working surface as shown in Table 2, a typical plate is made from a thickness of 10 mm, a scaling factor of one-half was chosen for all specified materials, resulting in specimens with a length of 250 mm. The thickness of the plate's ranges from 5.5 mm to 10.5 mm.

Manufacturing process

The resin serves as the matrix for fiberglass reinforcement, analogous to how concrete functions as the matrix for steel reinforcement bars, a critical aspect of this process is maintaining a fiber-to-matrix ratio of 50/50 by weight. which ensures optimal mechanical properties and structural integrity of the composite material, the manufacturing process employed contact molding in an open mold, which allows for precise layering of woven reinforcement in the prescribed order. A rigid plywood platform was selected as the base, providing stability and support during the molding process, to facilitate easy removal of the finished composite, a plastic sheet was placed on the plywood, and a thin film of polyvinyl alcohol was applied as a release agent using a spray gun, this step is crucial for preventing adhesion between the mold and the composite, ensuring a smooth finish, Laminating began with the application of a gel coat (composed of epoxy and hardener) brushed onto the mold. This gel coat serves two primary purposes: it provides a smooth outer surface that enhances the aesthetic quality of the finished product and protects the fibers from direct exposure to environmental factors. which could compromise their performance. Plies were meticulously cut from rolls of woven fabric. ensuring uniformity and consistency in the layers. The reinforcement layers were then carefully placed onto the mold over the gel coat. followed by the application of additional gel coat to enhance bonding and structural cohesion, to eliminate any trapped air that could weaken the composite, serrated steel rollers

Table 1. Test specimen material properties

Test specimen material properties	Magnesium AZ31B-O	CFRP 670 carbon 2 × 2 Twill	RFN/epoxy
Mass density	1.800 kg/m³	1.522 kg/m³	671 g/m² (0.671 kg/m²)
Elastic modulus $E_1 = E_2$	45 GPa	45.3 GPa	25–30 GPa (typical for epoxy)
In-plane shear modulus G_{12}	17 GPa	12.3 GPa	5–6 GPa (typical for epoxy)
In-plane poisson's ratio v_2	NA	0.3	0.35 (typical for epoxy)
Plate thickness	NA	5 mm (example)	< 5 mm
Fiber volume	52–56%	50–60%	N/A

Figure 1. Natural DISS Plant and Selected and Cut DISS Fibers

were employed, this step is vital, as it ensures complete compaction of the layers, leading to improved mechanical properties and durability of the final product [21].

Geometric properties

The selection of plate types for construction and testing focused on woven glass/epoxy composite plates. A total of seven woven fiber glass/epoxy composite plates were prepared for hand lay-up. Each plate has a maximum length of 250 mm, and the average thickness of all samples was measured using a micrometer with a minimum resolution of 0.01 mm. (Figure 3)

Experimental boundary conditions

The first boundary condition tested was a free boundary condition. which aimed to evaluate the damping characteristics of the materials, this condition simulates the free state of the plate. with no external dissipative forces acting on it. To achieve this, each plate was suspended using only thin wire.

Determination of material constants

The properties of the woven glass/epoxy composite plate can be characterized using two material constants: Young's modulus (E) and Poisson's ratio (ν), for this characterization. laminate consisting of eight layers was manufactured to evaluate these constants.

The material constants were determined experimentally through tensile tests conducted on specimens. following the ASTM standards D 638-08 and D 3039/D 3039M – 2006. Specimens were cut from the composite plates using diamond cutting tools or hexagonal saws and subsequently polished using a polishing machine, at least three repeated samples were analyzed, and average values were adopted for the material constants [22].

Test plate dimensions

Table 2 presents the dimensions of the test plates including material type, layup configuration edge length, thickness, and aspect ratio.

EXPERIMENTAL METHODOLOGY

Test setup

Figure 2 shows the setup used, the object, a square plate of multilayer composite material, is subjected to stress by a vibration pot capable of creating vibration or shock forces, whether steady state or transient, Vibration forces are used to vibrate the plate in one of its fundamental modes, to obtain a specific mode, the pot's stinger must be placed on the antinode of the desired mode, and the stress frequency must be the corresponding fundamental frequency, conversely, shock forces allow different modes to be visualized simultaneously, in this case, the stinger is placed at the center of the plate.

A network of parallel lines is projected onto the surface of an object using a video projector or slide projector, the object acts as a network phase shifter, analyzing the phase of this object network using a CCD camera allows the determination of its relief, a rotation system allows the complete relief of the object to be obtained (Figures 3, 4).

Table 2. Dimensions of the test plates

Plates	Material	Layup	Edge length (a, mm)	Thickness (t, mm)	Aspect ratio (a/t)
MAG I	AZ31B-O	NA	304.8	34.93	8.73
MAG II	AZ31B-O	NA	304.8	19.48	15.65
MAG III	AZ31B-O	NA	304.8	14.45	20.65
CFRP I	Quasi-Isotropic	(0/90/45/-45)	304.8	34.93	8.73
CFRP II	Quasi-Isotropic	(0/90/45/-45)	304.8	19.48	15.65
CFRP III	Cross Ply	(0/90)	304.8	14.45	20.65
FN/Epoxy I	F Diss	(0/90/45/-45)	304.8	34.93	8.73
FN/Epoxy II	F Diss	(0/90/45/-45)	304.8	19.48	15.65
FN/Epoxy III	F Diss	(0/90)	304.8	14.45	20.65
FN/Epoxy IV	F Diss	(0/90/45/-45)	304.8	34.93	8.73
FN/Epoxy V	F Diss	(0/90/45/-45)	304.8	19.48	15.65

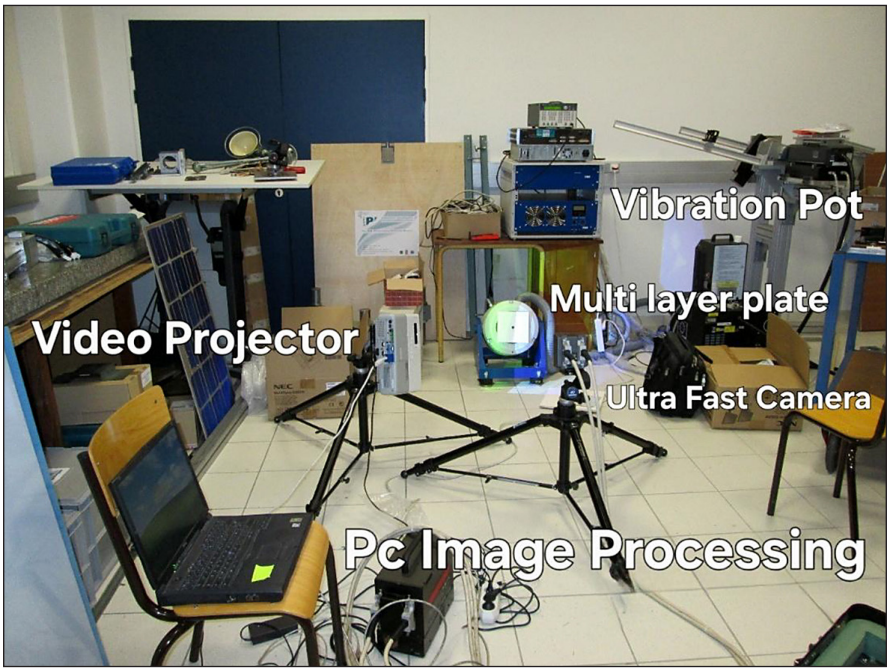

Figure 2. LMS setup for modal testing under free-free boundary conditions, showing the vibration pot, multilayer plate, optical projection system, and image processing unit

Optical measurement technique

A grid of parallel lines is projected onto the surface of the plate using a video projector or slide projector. allowing the object to act as a phase grating, the phase analysis of this projected grid. captured by a CCD camera. enables the determination of the surface relief, a rotational system is employed to achieve a complete relief profile of the plate (Figure 5). The plate's contours are designed to be free, as it is easier to establish free boundary conditions compared to fixed ones, the shaker used for this setup is TV50101 from Tira, with specifications detailed in Table 3.

Shadow interference measurement

In front of the plate, a reference grid is positioned, a shadow of this grid is projected onto the plate's surface by light emitted from a white light source, the geometric interference pattern between the reference grid and the shadowed grid is captured by a high-speed camera (Ultima APX Fastcam by Photron), capable of recording up to 2000 frames per second at full resolution and up to 100.000 frames per second at reduced resolution, The recorded fringe patterns are subsequently processed by a computer to extract displacement fields.

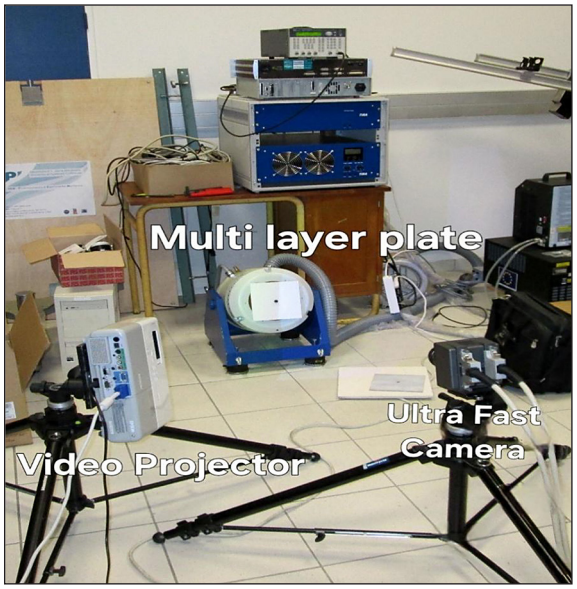

Figure 3. Experimental setup for modal testing of the multilayer plate under free boundary conditions using a video projector and ultra-fast camera for optical measurement

Test procedure

The resulting vibrations at a selected point on the plate are measured using an accelerometer, which is securely mounted with beeswax to ensure accurate reading, the accelerometer signal is then fed into the secondary channel of the analyzer, where its frequency spectrum is obtained, The response point is fixed at a specific location, while the excitation point is varied across the plate, Both input and output signals are analyzed using Fast Fourier Transform (FFT) techniques, allowing for the generation of frequency response functions (FRFs), These functions are transmitted to a computer for the extraction of modal parameters, The output from the analyzer is displayed on its screen using DEWESoft 6 software, facilitating direct measurement of various FRF shapes, This procedure is crucial for understanding the dynamic behavior of the composite plate and for validating the experimental setup.

Finite element modeling (ANSYS)

A finite element analysis (FEA) is performed on multilayer composite plates under free boundary conditions, using ANSYS software, the composite plate is modeled using the SHELL181 linear shell element, focusing on a modal analysis, the plate is assumed to have free boundaries, with degrees of freedom including UX, UY, UZ, ROTX, ROTY, and ROTZ. The model is constructed using 2D shell elements based on the edge length dimensions provided in Table 2, Five models are created with this geometry, each corresponding to a different plate thickness, the material model for the analysis adheres to the properties specified for the PRN plate, as outlined in Table 1, to simulate the constrained condition, distinct

Figure 4. a. Composite plate: Natural fiber composite oriented horizontally, b. Test specimens: Various cross-sectional shapes arranged vertically for evaluation

Table 3. Specifications of the Vibration Shaker

Parameters	Sinusoidal force	Random force	Shock force	Frequency	Displacement	Mass
Value	650 N	420 N	840 N	DC - 7000 Hz	25.4 mm	80 kg

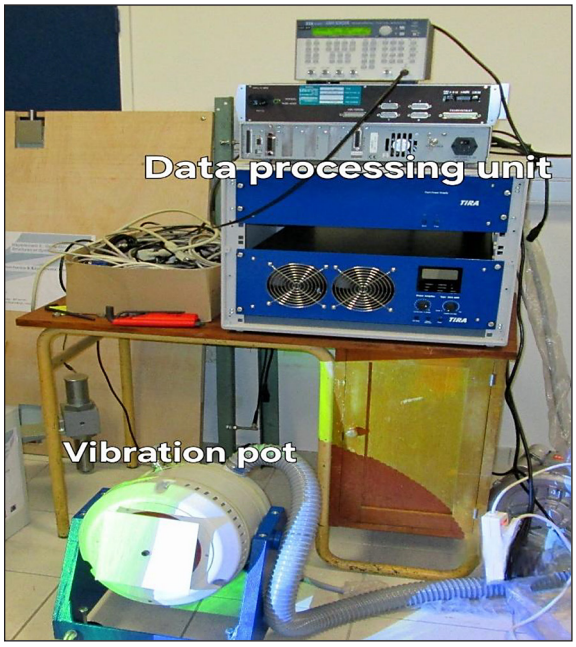

Figure 5. Vibration pot and data processing unit: Equipment setup for vibration testing and data analysis

boundary conditions are applied to the finite element model (FEM) Figure 6, SHELL181 is suitable for analyzing thin to moderately thick shell structures, It is a four-node element with six degrees of freedom at each node: translations in the x, y, and z directions, and rotations about the X, Y, and Z axes, If the membrane option is used, the element only has translational degrees of freedom, The degenerate triangular option should be used only as a filler element in mesh generation, SHELL181 can be employed for layered applications, modeling composite shells or sandwich constructions, the accuracy of composite shell modeling is governed by first-order shear deformation theory, commonly referred to as Mindlin-Reissner shell theory [23].

RESULTS AND VALIDATION

Finite element analysis

To establish baseline data and build confidence in the analytical and numerical results, an experimental study is conducted, Equation 5 provides the analytical frequency equation used to calculate the first five natural frequencies of an isotropic plate in free conditions [24].

$$f_n = \frac{\lambda_i^2}{2\pi a^2}\sqrt{\frac{Eh^3}{12\gamma(1-\upsilon^2)}} \tag{5}$$

where: f_n – the natural frequency of the plate (Hz), λ_i^2 – the frequency parameter associated with the i[th] mode shape, a – the plate length, E – the Young's modulus, h – the plate thickness, γ – the mass per unit area (often expressed as ρh\rho hρh), and ν – Poisson's ratio of the material.

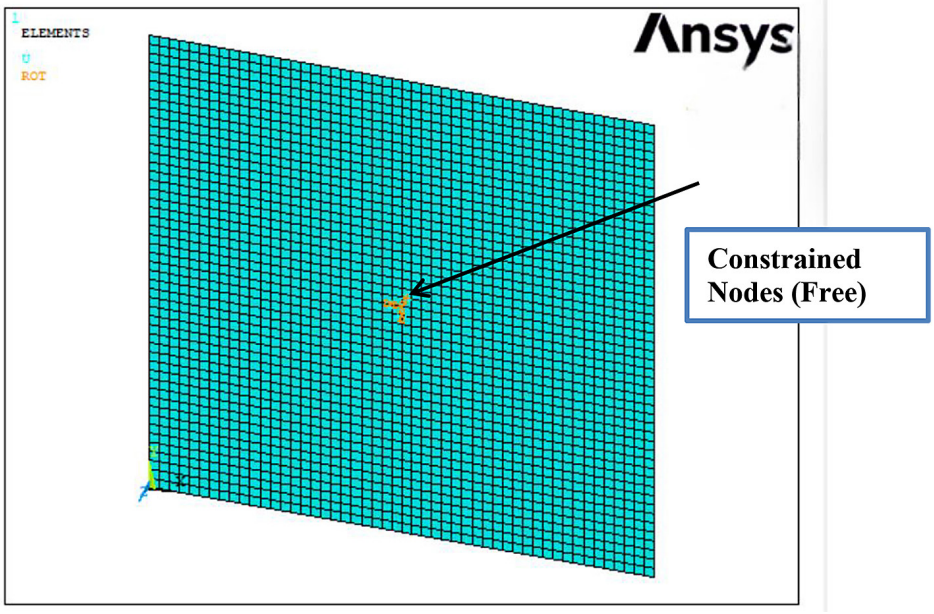

Figure 6. Finite element model of FN/Epoxy plaque free boundary conditions : Mesh representation for structural analysis in Ansys

The finite element model is employed to conduct a modal analysis on FN/Epoxy samples under free boundary conditions, with Figure 6 illustrating the first five mode shapes produced by the finite element method (FEM), These shapes are representative of the entire set of FN/Epoxy plates studied.

Natural frequencies derived from both the analytical equation and the FEM are compared with experimental results across all FN/Epoxy plates, Table 4 summarizes the first five unique natural frequencies for each method, facilitating a direct comparison, this analysis reveals a strong correlation, indicating that the FEM effectively captures the plates' dynamic behavior, notably, experimental natural frequencies tend to be lower than those predicted by analytical and FEM models, the majority of these differences are minimal, with all but two frequencies varying by less than 10%, Most experimental results show deviations of less than 8% from theoretical values, and many fall within 5% of the FEM results, bolstering confidence in the simulation's accuracy.

In scenarios involving bolted constrained boundary conditions, where closed-form solutions are unavailable, the focus shifts to comparing FEM and experimental outcomes, the two-dimensional plate model used for free conditions (illustrated in Figure 7) is adapted to analyze normal modes of the magnesium plate under constraints, boundary conditions in the FEM are implemented by first fixing certain nodes and then pinning others, Figure 5 depicts the first six mode shapes obtained from the fixed condition,

Table 4 presents the FEM and experimental results along with percentage differences for the experimental values under the constrained conditions, this data underscores the influence of these constraints on the calculated natural frequencies, especially for lower frequency modes, the results indicate that the pinned constraint consistently yields lower natural frequencies than the fixed condition, attributed to the decreased stiffness of the pinned plate, additionally, greater variability is observed in experimental results for pinned conditions compared to fixed ones, this finding suggests that the fixed boundary conditions in the model more closely represent the physical constraints for thinner plates, while thicker plates are designed to better mitigate the effects of pinning.

EXPERIMENTAL RESULTS

The tests on plates in free conditions served two primary objectives in this research, first, these tests aim to validate the accuracy of the FEM model, second, they provide a simple boundary condition

Table 4. Theoretical vs Experimental first natural frequencies for plates FN/Epoxy in the free condition

Plates	Experimental natural freq. (HZ)	Analytics % Diff	FEM % Diff
Plate I	1.110	-9.42	-2.26
	1.655	-7.72	-3.71
	2.077	-5.91	-5.92
	2.788		-3.51
	4.843	-12.35	-4.15
		-13.66	
Plate II	641	-6.84	-2.13
	952	-5.68	-2.76
	1.232	-3.31	-4.06
	1.642	-7.93	-3.01
	2.903	-7.11	-4.15
Plate III	492	-6.32	-3.03
	731	-5.07	-4.05
	920	-2.84	-2.82
	1.263	-6.74	-4.24
	2.251	-5.62	-2.86
Plate IV	441	-6.52	-4.29
	657	-5.64	-2.87
	834	-3.27	-4.61
	1.146	-6.90	-3.28
	2.025	-6.75	-5.23
Plate V	293	-7.30	-4.26
	428	-6.72	-4.46
	546	-4.04	-5.72
	742	-7.34	-4.54
	1.326	-7.31	-6.93

Table 5. Modal data arranged in order of mode shape

Plates	Modes	Shapes	Magnesium	CFRP	Parameter	RFN/Epoxy	RFN/Epoxy// CFRP
			Freq (Hz)	Freq (Hz)	Freq (%) Diff	Freq (Hz)	Freq (%) Diff
I	1	+	1113	621	-44.2	1.110	-44.0
	2	X	1664	1981	19.1	1.655	19.3
	3	O	2095	2042	-2.5	2.077	-2.2
	4	H	2797	2274	-18.7	2788	-18.5
	5	≠	4841	3393	-29.9	4843	-29.4
	6	SSS	4857	4389	-9.6	4853	-9.4
	7	*	5253	4538	-13.6	5251	-13.2
	8	O+	5914	4646	-21.4	5911	-21.3
II	1	+	639	618	-3.3	641	3.12
	2	X	949	985	3.8	952	-3.16
	3	O	1201	1205	0.3	1232	25.81
	4	H	1639	1571	-4.1	1642	1.83
	5	SSS	2906	2851	-1.9	2.903	-1.03
	6	≠	2959	2693	-9.0	2961	0.675
	7	*	3216	3034	-5.4	3212	-1.243
	8	O+	3620	3321	-8.3	3623	0.828
III	1	+	491	293	-40.3	492	-40.7
	2	X	728	942	29.4	731	29.6
	3	O	922	1032	11.9	920	11.2
	4	H	1268	1088	-14.2	1.263	-14.1
	5	SSS	2255	2432	7.8	2.251	7.5
	6	≠	2294	1780	-22.4	2291	-22.2
	7	*	2507	2512	0.2	2503	0.3
	8	O+	2817	2794	-0.7	2813	-0.5
IV	1	+	443	416	-6.1	441	-6.2
	2	X	655	751	14.7	657	14.5
	3	O	830	881	6.1	834	6.3
	4	H	1145	1133	-1.0	1.146	-1.2
	5	≠	2024	2157	6.6	2.025	6.5
	6	SSS	2080	1966	-5.5	2083	-5.2
	7	*	2263	2317	2.4	2262	2.3
	8	O+	2547	2500	-1.8	2543	-1.6
V	1	+	291	244	-16.2	293	-16.1
	2	X	429	473	10.3	428	10.2
	3	O	545	581	6.6	546	6.5
	4	H	755	683	-9.5	742	-9.8
	5	≠	1327	1304	-1.7	1.326	-1.9
	6	SSS	1382	1229	-11.1	1381	-11.3
	7	*	1499	1470	-1.9	1495	-1.7
	8	O	1681	1689	0.5	1683	0.4

Note: + – The nodal lines form a plus sign, X – The nodal lines form an X, O – The nodal lines form a ring shape, H – The nodal lines form a hyperbolic shape, SSS – The nodal lines form three sinusoids (the four edges of the plate have a complete sinusoid of displacement), * – The nodal lines form a shape of type *, O+ – The nodal lines are a superposition of the "O" and "+" shapes.

that allows for the comparison of the two materials, Table 5 presents data generated from the experimental mode, along with the structure described in Figure 8, which illustrates the frequency rates of the first eight unique modes, Figure 7 shows the experimental mode shapes for the first eight modes listed in Table 5, the nomenclature used to describe these mode shapes in the tables is as follows:

To enhance the accuracy of model validation, a quantitative correlation between the experimental and FEM results was established. The comparison yielded a high coefficient of determination ($R^2 = 0.984$) and an average deviation of approximately 3.5%, confirming the strong agreement between experimental data and numerical simulations. These findings validate the reliability of the FEM model in predicting the dynamic behavior of composite structures under free-free boundary conditions.

The data for CFRP (carbon fiber reinforced polymer) are organized according to the corresponding magnesium mode shapes rather than by frequency, this arrangement reflects the observation that CFRP mode shapes may appear in a different sequence than those of magnesium, owing to material anisotropy, examining the percentage differences in Table 6 provides several key insights, specifically, the first natural frequency

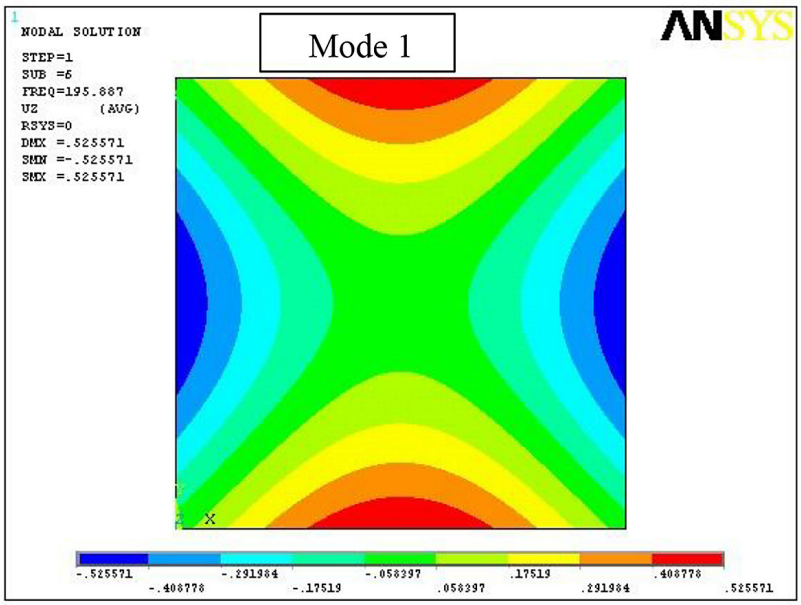
NODAL SOLUTION
STEP=1
SUB =6
FREQ=195.887
UZ (AVG)
RSYS=0
DMX =.525571
SMN =-.525571
SMX =.525571
Mode 1
ANSYS
-.525571
-.408778
-.291984
-.17519
-.058397
.058397
.17519
.291984
.408778
.525571

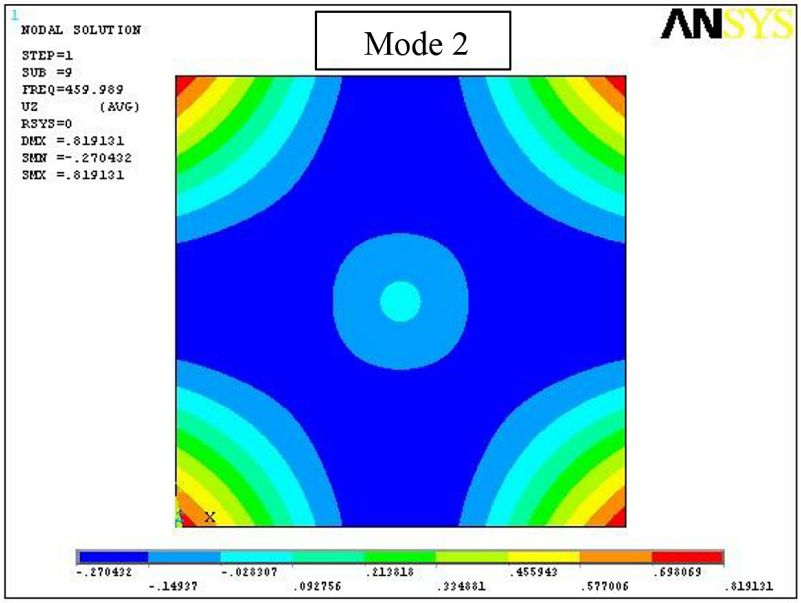
NODAL SOLUTION
STEP=1
SUB =9
FREQ=459.989
UZ (AVG)
RSYS=0
DMX =.819131
SMN =-.270432
SMX =.819131
Mode 2
ANSYS
-.270432
-.14937
-.028307
.092756
.213818
.334881
.455943
.577006
.698069
.819131

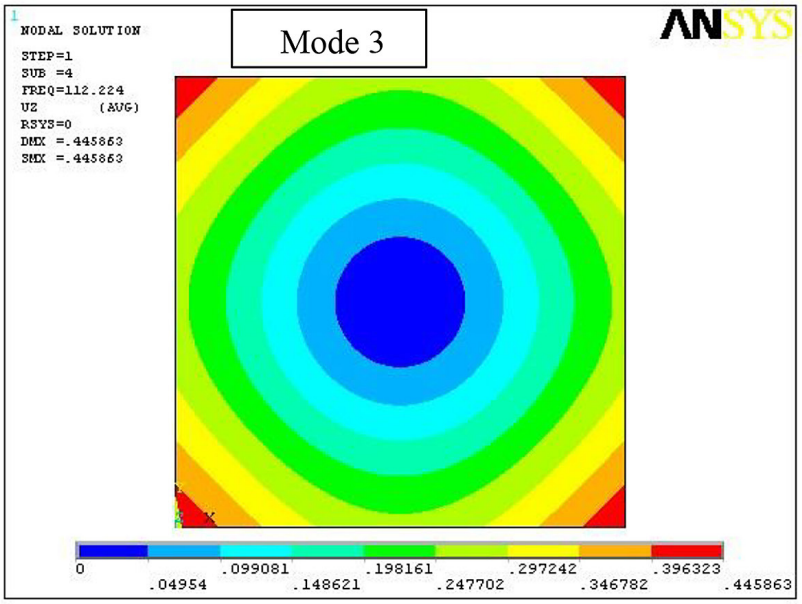
NODAL SOLUTION
STEP=1
SUB =4
FREQ=112.224
UZ (AVG)
RSYS=0
DMX =.445863
SMX =.445863
Mode 3
ANSYS
0
.04954
.099081
.148621
.198161
.247702
.297242
.346782
.396323
.445863

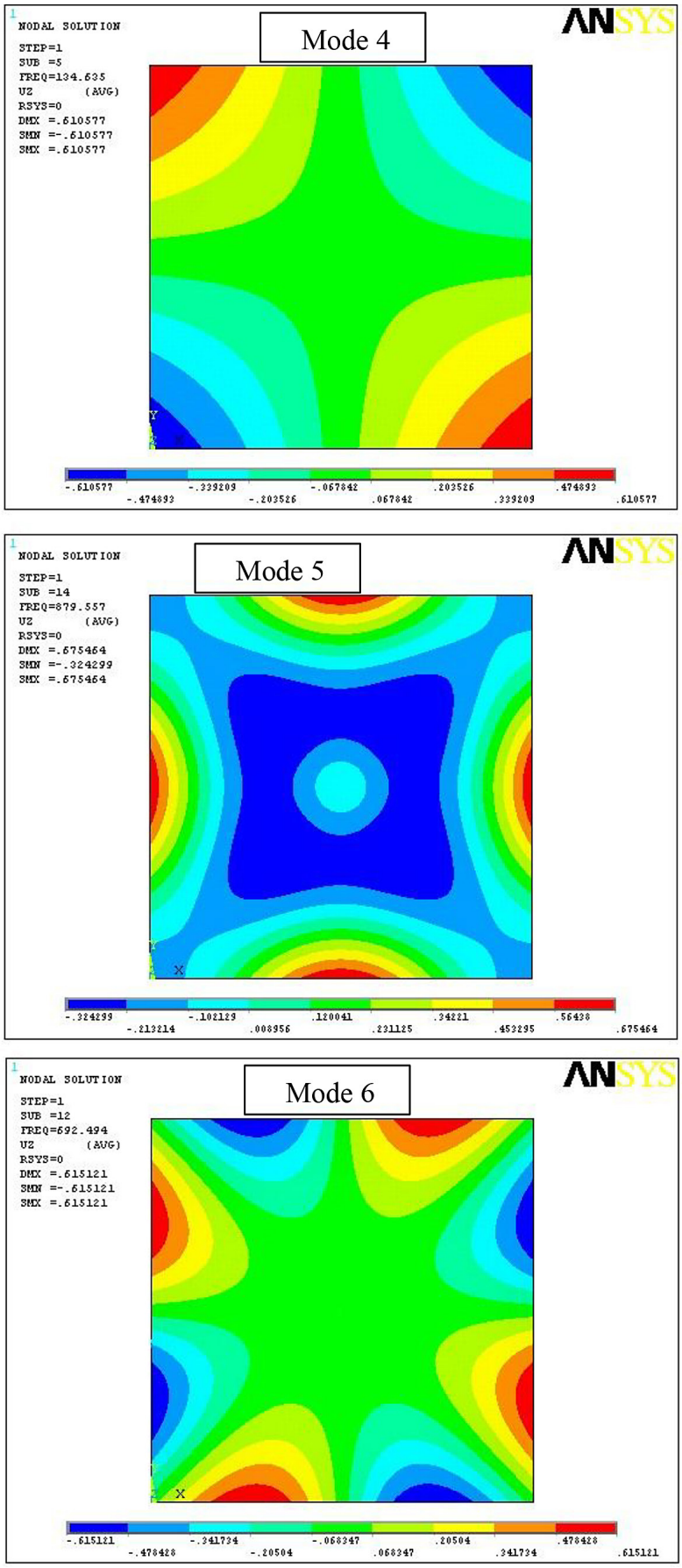

Figure 7. First six mode shapes of FN/Epoxy II: Visualization of the vibrational modes in free condition, illustrating the distinct patterns of deformation at various frequencies

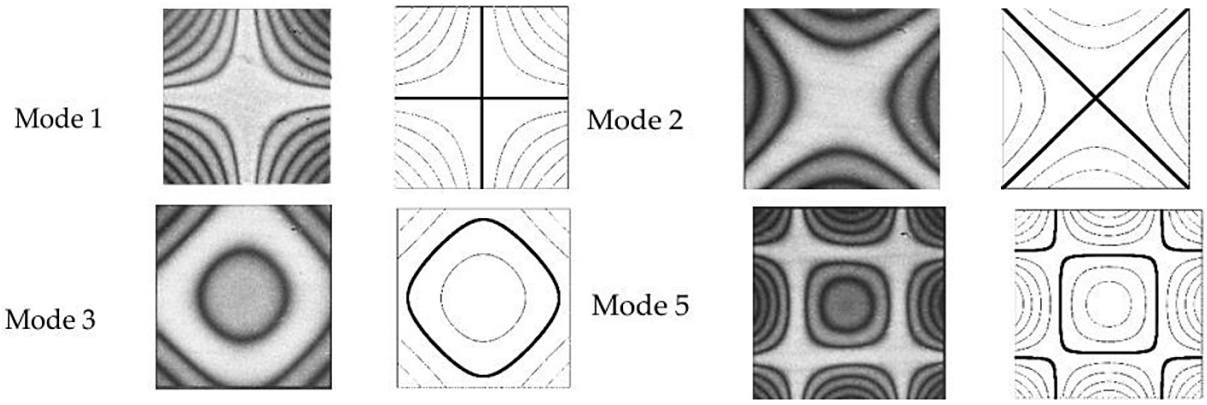

Figure 8. Frequency rates of the first four unique modes [25]

of CFRP I is 44.2% lower than that of MAG I, while the second mode is 19.1% higher, indicating that frequency ordering is not preserved across materials, moreover, CFRP I exhibits a significant frequency gap between the first and second modes, a feature attributed to transverse shear effects and direction-dependent stiffness in composite laminates.

Figure 6 illustrates the frequency response of the MAG I and CFRP I specimens, highlighting these mode sequence differences. Notably, CFRP I demonstrates substantially higher damping compared to magnesium – approximately 1000% higher for the first mode and 290% higher for the second – confirming its superior vibration attenuation capabilities,

The influence of aspect ratio and fiber orientation further explains the observed frequency shifts, As the aspect ratio increases, the bending stiffness decreases, leading to lower natural frequencies, especially in the lower-order modes where bending dominates, Conversely, specimens with reduced aspect ratios exhibit higher stiffness and thus elevated natural frequencies, Fiber orientation plays a crucial role in this behavior: unidirectional laminates tend to concentrate stiffness along the fiber axis, elevating frequencies in the corresponding bending directions, while cross-ply configurations distribute stiffness more evenly, resulting in mixed or shifted mode shapes.

Figure 8 presents the natural frequencies of all specimens under free-free boundary conditions, Frequency variations are more pronounced in thinner samples; as thickness increases, these discrepancies diminish, For Specimens II and IV, natural frequency differences remain within ±9%, indicating good consistency between experimental and FEM predictions, In contrast, Specimen V shows slightly larger deviations, while the most significant difference (–16.2%) is observed in CFRP III, the only specimen featuring cross-ply layers, This variation stems from the non-isotropic elastic properties of the laminate, which alter the stiffness distribution and shift mode shapes compared to isotropic magnesium.

Figure 7 also depicts the modal damping ratios for the first eight modes across all samples, expressed as percentages of critical damping, the visualization underscores the substantial damping enhancement in CFRP compared to magnesium, aligning with the expected behavior of anisotropic polymer-matrix composites [26–27].

The investigation into the natural frequencies of woven glass/epoxy composite plates reveals that the natural frequency increases with the aspect ratio, following a parabolic trend consistent with theoretical predictions, Higher aspect ratios enhance stiffness and reduce mass per unit area, resulting in elevated natural frequencies, Natural frequencies were measured using a data acquisition system under free boundary conditions, focusing on three parameters: aspect ratio, fiber orientation, and sample preparation, A finite element analysis (FEA) program was developed to compare experimental values with theoretical results, The findings indicate that natural frequencies sometimes vary within a certain range, suggesting good agreement with FEA predictions, As the mode number increases, the percentage error between experimental values and simulation results decreases, indicating that higher modes are less sensitive to inaccuracies, However, discrepancies arise because the analytical models consider only undamped natural frequencies, while real systems exhibit inherent damping, leading to variations between

Table 6. Constrained modal data arranged in order of mode shape

Plates	Modes	Shapes	Magnesium	CFRP	Parameter	RFN/Epoxy	RFN/Epoxy// CFRP
			Freq (Hz)	Freq (Hz)	Freq % Diff	Freq (Hz)	Freq % Diff
I	1	+	1885	2029	7.6	2026	7.2
	2	X	2104	1184	-43.7	1187	-43.5
	3	O	2138	2148	0.5	2151	0.3
	4	H	2274	NA	NA	NA	NA
	5	≠	2864	NA	NA	NA	NA
	6	SSS	2932	2310	-21.2	2308	-21.4
	7	*	4868	3400	-30.2	3404	-30.3
	8	O+	5350	4556	-14.8	4553	-14.6
II	1	+	1281	1077	-15.9	1072	-15.5
	2	X	1416	1256	-11.3	1252	-11.4
	3	O	1444	NA	NA	NA	NA
	4	H	1706	1314	-23.0	1317	-23.2
	5	SSS	1811	1661	-8.3	1664	-8.5
	6	≠	2440	1770	-27.5	1768	-27.4
	7	*	2999	2707	-9.7	2702	-9.2
	8	O+	3398	3085	-9.2	3081	-9.4
III	1	+	1125	1041	-7.5	1045	-7.3
	2	X	1224	NA	NA	NA	NA
	3	O	1243	1119	-10.0	1121	-10.2
	4	H	1422	1100	-22.6	1105	-22.3
	5	SSS	1501	1268	-15.5	1264	-15.1
	6	≠	2050	1700	-17.1	1701	-17.3
	7	*	2354	1801	-23.5	1805	-23.2
	8	O+	2764	2687	-2.3	2684	-2.1
IV	1	+	989	805	-18.6	802	-18.2
	2	X	1100	NA	NA	NA	NA
	3	O	1153	1002	-13.1	1006	-13.3
	4	H	1273	1066	-16.3	1062	-16.1
	5	≠	1383	1202	-13.1	1204	-13.4
	6	SSS	1837	1583	-13.8	1582	-13.5
	7	*	2130	1977	-7.2	1975	-7.1
	8	O+	2501	2383	-4.7	2386	-4.5
V	1	+	753	677	-10.1	676	-10.2
	2	X	NA	735	NA	737	NA
	3	O	833	765	-8.2	762	-8.3
	4	H	921	795	-13.7	797	-13.5
	5	≠	996	867	-13.0	863	-13.2
	6	SSS	1295	1196	-7.6	1195	-7.3
	7	*	1433	1277	-10.9	1273	-10.4
	8	O+	1503	1487	-1.1	1485	-1.3

experimental measurements and simulations, Factors contributing to observed discrepancies include the dog-bone-shaped specimen geometry, which may induce variability in elastic properties, and fluctuations in tensile properties due to sample preparation methods and testing conditions, Additionally, the specimens did not always align at the center of the jaws during testing due to a diamond-shaped hole, which could result in a reduction of the Young's modulus, Overall, these findings highlight the importance of geometric considerations in design and underscore the need for improved specimen preparation techniques and alignment during testing to enhance accuracy in vibrational property measurements, ultimately leading to better design practices for composite materials in engineering applications [28–30] (Figure 9).

The investigation into the natural frequencies of woven glass/epoxy composite plates reveals that the natural frequency increases with the aspect ratio, following a parabolic trend consistent with theoretical predictions, higher aspect ratios enhance stiffness and reduce mass per unit area, resulting in elevated natural frequencies, natural frequencies were measured using a data acquisition system under free boundary conditions, focusing on three parameters: aspect ratio, fiber orientation, and sample preparation, a FEA program was developed to compare experimental values with theoretical results, (Figure 10).

The findings indicate that natural frequencies sometimes vary within a certain range, suggesting good agreement with FEA predictions, As the mode number increases, the percentage error between experimental values and

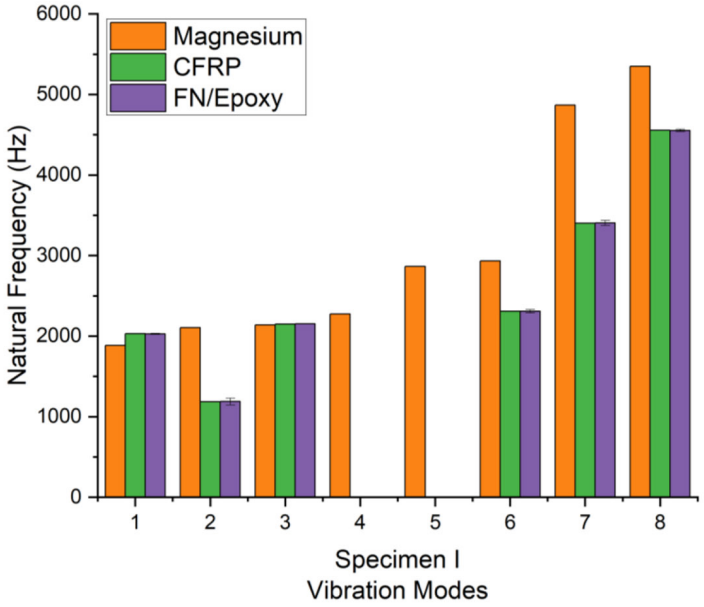
Magnesium
CFRP
FN/Epoxy
Natural Frequency (Hz)
0
1000
2000
3000
4000
5000
6000
1
2
3
4
5
6
7
8
Specimen I
Vibration Modes

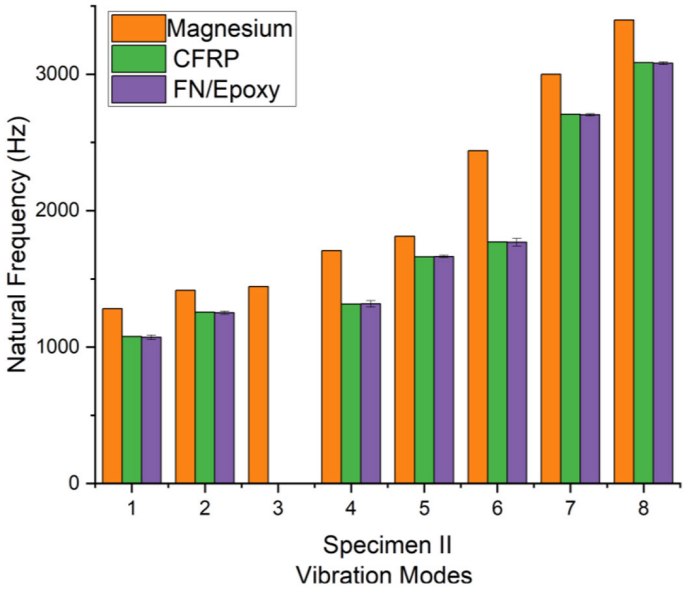
Magnesium
CFRP
FN/Epoxy
Natural Frequency (Hz)
0
1000
2000
3000
1
2
3
4
5
6
7
8
Specimen II
Vibration Modes

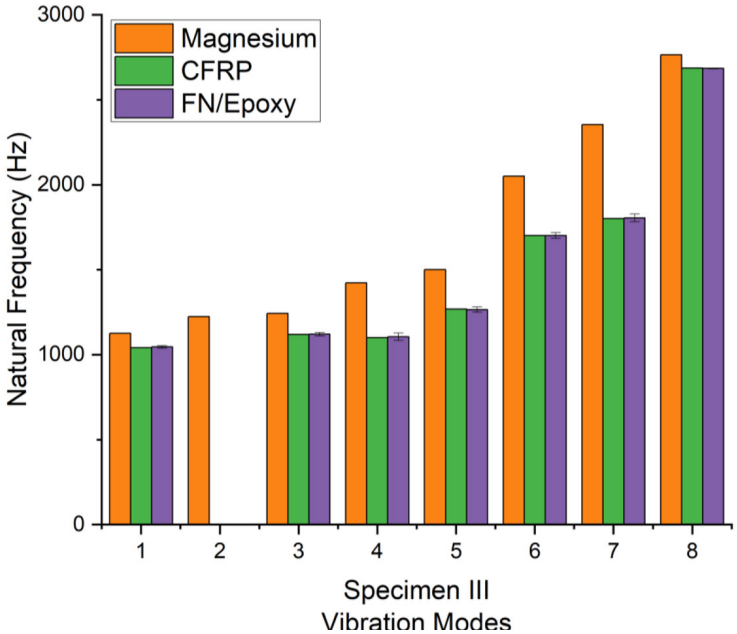
Magnesium
CFRP
FN/Epoxy
Natural Frequency (Hz)
0
1000
2000
3000
1
2
3
4
5
6
7
8
Specimen III
Vibration Modes

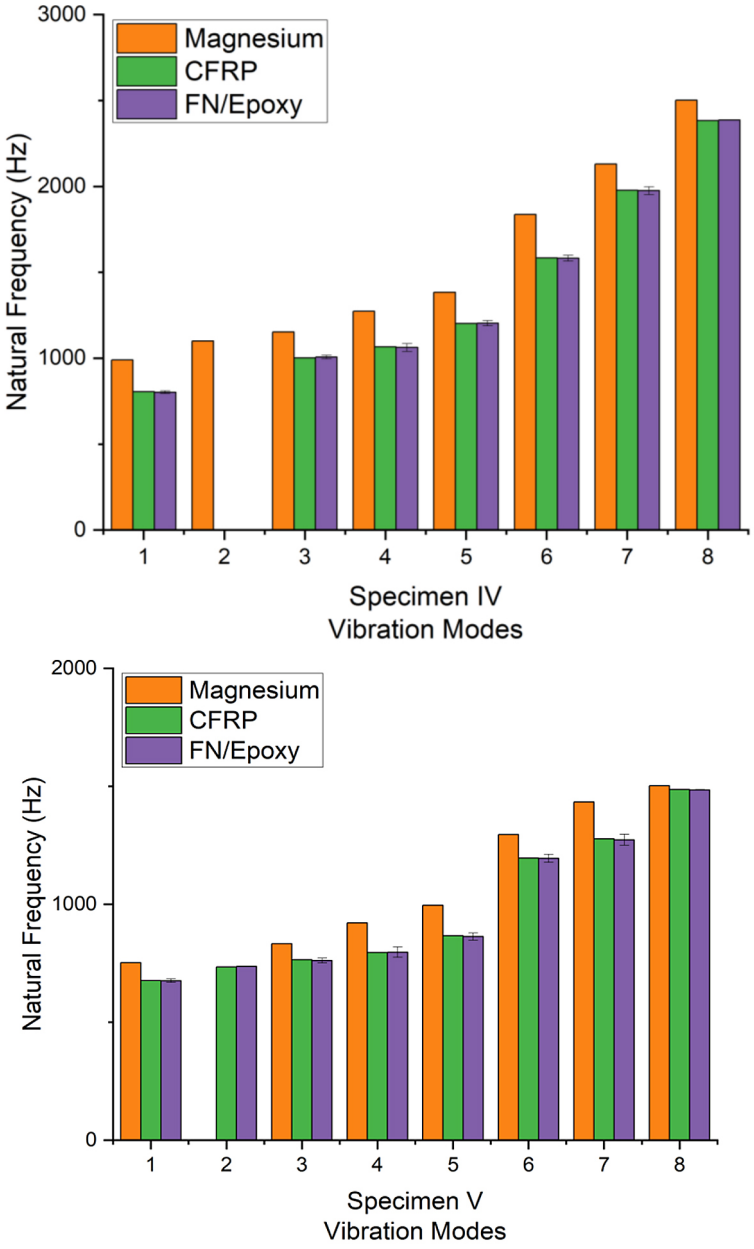

Figure 9. The 1st eigh Free Modal Natural Frequencies for each plate

simulation results decreases, indicating that higher modes are less sensitive to inaccuracies, however, discrepancies arise because the analytical models consider only undamped natural frequencies, while real systems exhibit inherent damping, leading to variations between experimental measurements and simulations, factors contributing to observed discrepancies include the dog-bone-shaped specimen geometry, which may induce variability in elastic properties, and fluctuations in tensile properties due to sample preparation methods and testing conditions, additionally, the specimens did not always align at the center of the jaws during testing due to a diamond-shaped hole, which could result in a reduction of the elastic modulus (Young's modulus), Overall, these findings highlight the importance of geometric considerations in design and underscore the need for improved specimen preparation techniques and alignment during testing to enhance accuracy in vibrational property measurements, this ultimately leads to better design practices for composite materials in engineering applications.

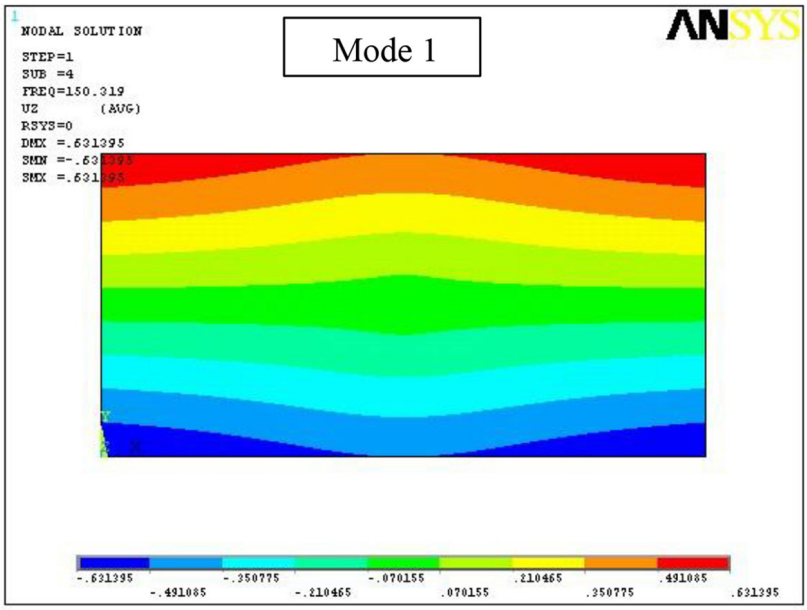
NODAL SOLUTION
STEP=1
SUB =4
FREQ=150.319
UZ (AVG)
RSYS=0
DMX =.631395
SMN =-.631395
SMX =.631395
Mode 1
ANSYS
-.631395
-.491085
-.350775
-.210465
-.070155
.070155
.210465
.350775
.491085
.631395

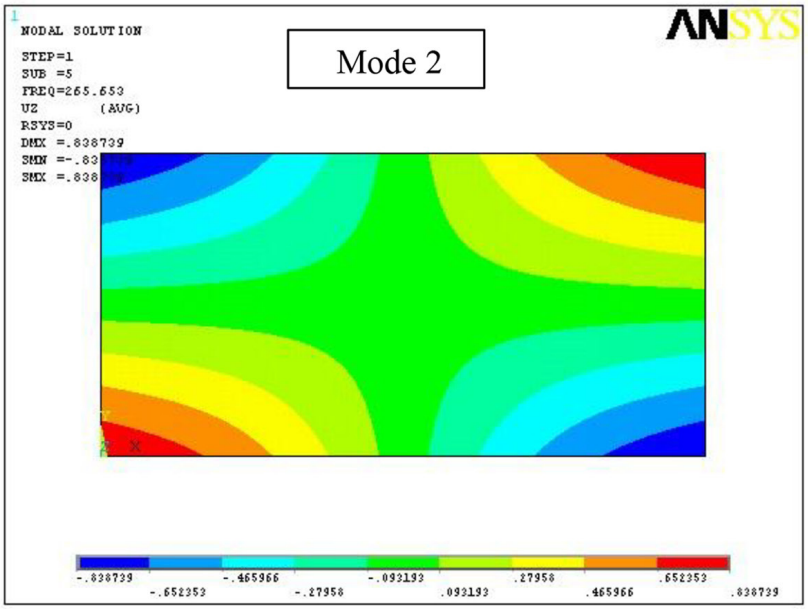
NODAL SOLUTION
STEP=1
SUB =5
FREQ=265.653
UZ (AVG)
RSYS=0
DMX =.838739
SMN =-.838739
SMX =.838739
Mode 2
ANSYS
-.838739
-.652353
-.465966
-.27958
-.093193
.093193
.27958
.465966
.652353
.838739

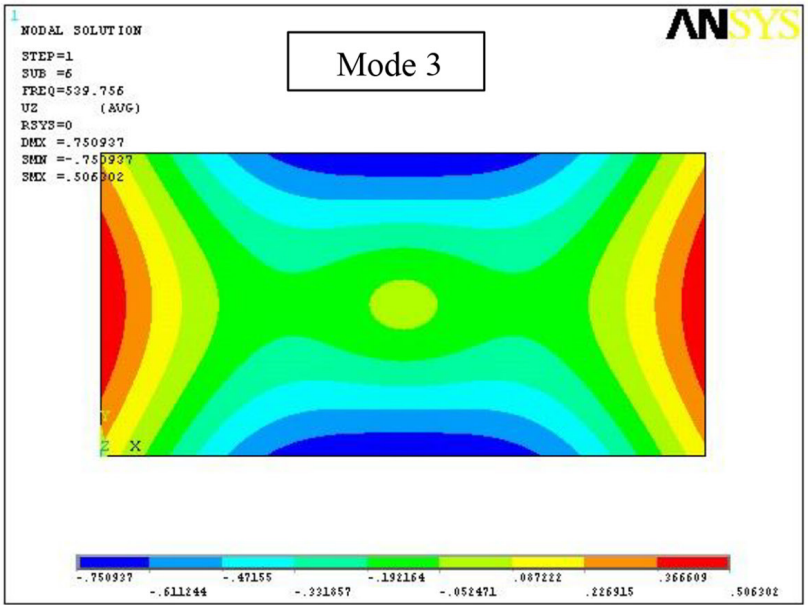
NODAL SOLUTION
STEP=1
SUB =6
FREQ=539.756
UZ (AVG)
RSYS=0
DMX =.750937
SMN =-.750937
SMX =.506302
Mode 3
ANSYS
-.750937
-.611244
-.47155
-.331857
-.192164
-.052471
.087222
.226915
.366609
.506302

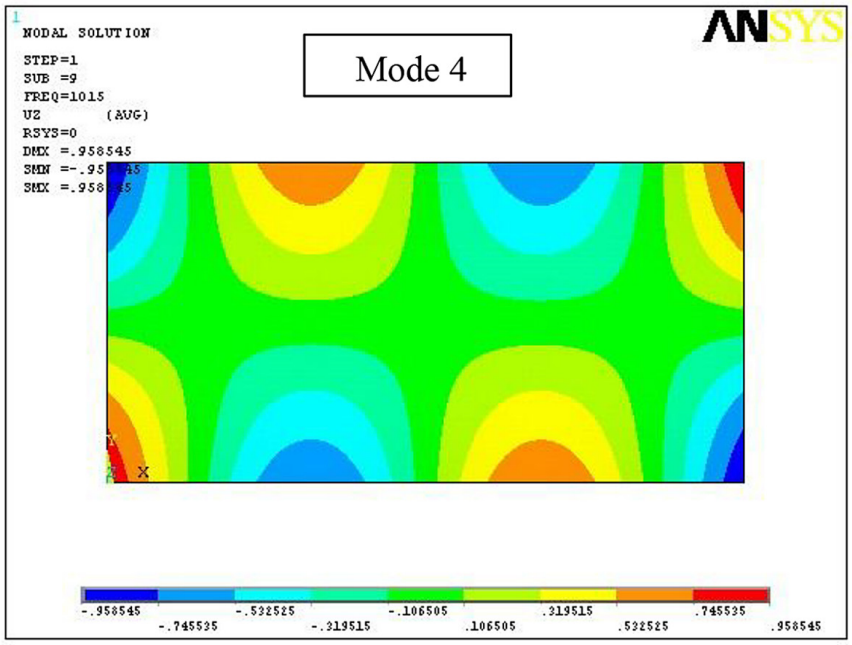

Figure 10. Natural modes of multilayer composite plates: Visualization of vibrational modes showing distinct deformation patterns

CONCLUSIONS

This research investigated the modal behavior of woven glass/epoxy and natural fiber/epoxy composite plates under free boundary conditions using an optical data acquisition system, Frequency response functions were extracted through fast Fourier transform (FFT) analysis, enabling precise characterization of vibrational modes, the results demonstrated that both aspect ratio and fiber orientation significantly influence the natural frequencies of the plates, Experimental results showed strong agreement with ANSYS simulations, with percentage errors below 15%, primarily attributed to uncertainties in elastic material properties, natural frequencies increased with aspect ratio, reflecting the combined effects of higher stiffness and reduced mass, while frequency variation with fiber orientation followed a non-linear trend – decreasing up to [45/−45] and rising again at [0/90], this highlights the complex coupling between material anisotropy and geometric configuration, from an industrial standpoint, the findings underscore the suitability of hybrid natural fiber composites for lightweight dynamic structures such as rotorcraft panels, UAV frames, and vibration-damping systems in aerospace and automotive applications, these materials offer a sustainable alternative to conventional composites without compromising structural performance, future research will extend this work toward constrained boundary conditions, evaluate fatigue life, and include full-scale component testing to validate the material's long-term durability and performance in operational environments.

REFERENCES

1. Zhang, Q., Adam, N.C., Hosseini Nasab, S.H. et al. Techniques for in vivo measurement of ligament and tendon strain: A review. Ann Biomed Eng 2021; 49, 7–28. https://doi.org/10.1007/s10439-020-02635-5
2. Alarifi, I. M. Revolutionising fabrication advances and applications of 3D printing with composite materials: a review. Virtual and Physical Prototyping, 2024; 19(1). https://doi.org/10.1080/17452759.2024.2390504
3. Pîrvu, C. I., Sover, A., Abrudeanu, M. Participation of polymer materials in the structure of piezoelectric composites. Polymers, 2024; 16(24), 3603. https://doi.org/10.3390/polym16243603
4. Tai, J. L., Sultan, M. T. H., Łukaszewicz, A., Józwik, J., Oksiuta, Z., Shahar, F. S. Recent trends in non-destructive testing approaches for composite materials: A review of successful implementations. Materials, 2025; 18(13), 3146. https://doi.org/10.3390/ma18133146

5. Omiogbemi, I. M. B., Awode, E. I., Muhammad, M. H., Adesanmi, A., Dagwa, I. M. Smart Composite Materials for Aerospace Applications. Functional Composites: Role in Modern Engineering, 2025; 115–168. https://doi.org/10.1002/9781394242030.ch6
6. Mazarbhuiya, R. M., Veeman, D. A comprehensive review on free vibrational analysis of natural fibers reinforced composite materials. Journal of Reinforced Plastics and Composites, 2025. https://doi.org/10.1177/07316844251364331
7. Şimşir, E., Akçin Ergün, Y., Yavuz, İ. Investigation of damping properties of natural fiber-reinforced composites at various impact energy levels. Polymers, 2024; 16(24), 3553. https://doi.org/10.3390/polym16243553
8. Khalid, M. Y., Al Rashid, A., Arif, Z. U., Ahmed, W., Arshad, H., Zaidi, A. A. Natural fiber reinforced composites: Sustainable materials for emerging applications. Results in Engineering, 2021; 11, 100263. https://doi.org/10.1016/j.rineng.2021.100263
9. Kumar, P., Singh, R., Verma, S. Free vibration behavior of natural and hybrid fiber composites: A review. Composite Structures, 2023; 305, 116589. https://doi.org/10.1016/j.compstruct.2023.116589
10. Singh, R., Nayak, S., Hegde, S., Padmaraj, N. H. Influence of fiber length and moisture content on sound and vibration characteristics of hemp/epoxy composites. Journal of Applied Engineering Science, 2023; 21(3), 957–962. https://doi.org/10.5937/jaes0-44872
11. Islam, M. S., Rahman, M. M., Alam, M. N. A review on hybrid natural fiber composites: Mechanical and dynamic performance. Renewable Materials Journal, 2024; 2(1), 45–62.
12. Boudjaada, Y., Benmansour, T., Fiala, H. E., Issasfa, B. Experimental and numerical investigation of the honeycomb structures' effect on the dynamic characteristics of rotors: a modal analysis. The International Journal of Advanced Manufacturing Technology, 2024; 133(9), 4453–4467. https://doi.org/10.1007/s00170-024-13875-3
13. Rathod, V. P., Wankhade, S. H. A review on impact of micro-tools on micro-milling outcomes for aluminium alloy. Advances in Science and Technology. Research Journal, 2025; 19(3). https://doi.org/10.12913/22998624/200007
14. Rathod, V. P., Wankhade, S. H. Comprehensive review of tool treatments and innovations in micro-milling precision and performance. Advances in Science and Technology. Research Journal, 2025; 19(4). https://doi.org/10.12913/22998624/200545
15. Kamble, Y. G., Rajiv, B., Rathod, V. P., Pantawane, P., Wankhade, S. Center drill geometry mapping in friction drilling of aluminium 6063 using artificial neural network approach. Advances in Science and Technology. Research Journal, 2025; 19(11). https://doi.org/10.12913/22998624/209120
16. Rathod, V. P., Wankhade, S. H., Kamble, Y. G. Experimental analysis of process parameters in micro-milling of AA6063-T6 using 7% cobalt WC tools. Advances in Science and Technology. Research Journal.
17. Rathod, V. P., Wankhade, S. H., Kamble, Y. G. Evaluating the Efficiency of Micro End Mill Tools and Performance Metrics in Micro Milling. Journal of Mines, Metals and Fuels, 2025; 73(7), 2253–2265. https://doi.org/10.18311/jmmf/2025/49414
18. Montalvao, D., Maia, N. M. M., Ribeiro, A. M. R. A review of vibration-based structural health monitoring with special emphasis on composite materials. Shock and vibration digest, 2006; 38(4), 295–324. https://doi.org/10.1177/0583102406065898
19. Omiogbemi, I. M. B., Awode, E. I., Muhammad, M. H., Adesanmi, A., Dagwa, I. M. (2025). Smart composite materials for aerospace applications. Functional Composites: Role in Modern Engineering, 115–168. https://doi.org/10.1002/9781394242030.ch6
20. Singh, K. K., Shrivastava, R. Influence of fiber orientation on thermo-mechanical response of symmetric glass/epoxy composite. Journal of the Brazilian Society of Mechanical Sciences and Engineering, 2023; 45(6), 288. https://doi.org/10.1007/s40430-023-04228-4
21. Diniță, A., Ripeanu, R. G., Ilincă, C. N., Cursaru, D., Matei, D., Naim, R. I., ..., Portoacă, A. I. Advancements in fiber-reinforced polymer composites: a comprehensive analysis. Polymers, 2023; 16(1), 2. https://doi.org/10.3390/polym16010002
22. Barbero, E., Fernández-Sáez, J., Navarro, C. Statistical analysis of the mechanical properties of composite materials. Composites Part B: Engineering, 2000; 31(5), 375–381. https://doi.org/10.1016/S1359-8368(00)00027-5
23. David Müzel, S., Bonhin, E. P., Guimarães, N. M., Guidi, E. S. Application of the finite element method in the analysis of composite materials: A review. Polymers, 2020; 12(4), 818. https://doi.org/10.3390/polym12040818
24. Daş, O., Daş, D. B. Free vibration analysis of isotropic plates using regressive ensemble learning. Avrupa Bilim ve Teknoloji Dergisi, 2022; (38), 428–434. https://doi.org/10.31590/ejosat.1135944
25. Hoksbergen. J.S. Ramulu. M. Reinhall. P. et al. A comparison of the vibration characteristics of carbon fiber reinforced plastic plates with those of magnesium plates. Appl Compos Mater 2009; 16, 263–283. https://doi.org/10.1007/s10443-009-9093-7
26. Zhang, J., Rao, J., Ma, L., Wen, X. Investigation of the Damping Capacity of CFRP Raft

Frames. Materials, 2022; 15(2), 653. https://doi.org/10.3390/ma15020653

27. Navaneeth, I. M., Poojary, S., Chandrashekar, A., Razak, A., Hasan, N., Almohana, A. I. Damped free vibration analysis of woven glass fiber-reinforced epoxy composite laminates. Advances in materials Science and Engineering, 2022(1); 6980996. https://doi.org/10.1155/2022/6980996
28. Chavan, S. S., Joshi, M. M. Study on vibration analysis of composite plate. International journal of advances in Production and Mechanical Engineering, 2015; 1(4).
29. Jafari, A., Kazemian, A. H., Rahmani, H. Investigating of vibration properties of aluminum plates in radii of different curvatures reinforced with glass fibers by modal analysis method experimentally and numerically. Fibers and Polymers, 2024; 25(4), 1457–1478. https://doi.org/10.1007/s12221-024-00503-w
30. Huang, Y.-H., Yen, C.-Y., Huang, T.-R. Dynamic non-destructive evaluation of piezoelectric materials to verify on accuracy of transversely isotropic material property measured by resonance method. Applied Sciences, 2020; 10(15), 5072. https://doi.org/10.3390/app10155072